

# Annealing of Pt-H Defects in High-Voltage Si p+/n- Diodes

Fabian Rasinger,\* Jennifer Prohinig, Holger Schulze, Hans-Joachim Schulze, and Gregor Pobegen

**A sophisticated way to adjust the minority carrier lifetime and, therefore, the reverse recovery charge in silicon (Si) power diodes is doping with platinum (Pt), as deep levels within the silicon bandgap are created. However, additional deep levels are introduced by hydrogen-incorporating processes during the fabrication of these diodes, which are caused by platinum–hydrogen (Pt–H) defects. Herein, the focus is on how Pt–H defects influence the p+/n- diode characteristics at reverse biasing and verify that annealing at temperatures higher than 300 K decreases the concentration of these defects to a minimum. The dissociation energy of this annealing process is obtained by assuming a first-order reaction. Furthermore, depth profiles of the Pt–H defect are calculated via current–voltage (IV) characteristics. Not only the impact of the Pt–H defect on the device performance is in a reverse direction but also its controllability via thermal annealing in a conventional furnace is presented.**

the formation of the H-decorated Pt sites in the Si crystal, e.g., Pt–H or Pt–H<sub>x</sub>.<sup>[9,10]</sup> These defects are generating several electrical active energy levels within the Si bandgap, which can drastically change the device characteristics. Sometimes other transition metals (TM)<sup>[11–14]</sup> instead of Pt are used for minority carrier lifetime engineering. Through density functional theory calculations of several TM–H<sub>x</sub>,<sup>[15]</sup> it has been possible to connect electrically active defect levels with the microscopic point defect type.

The applicability of deep-level transient spectroscopy (DLTS) for trap-level characterization on fully fabricated p+/n- diodes designed for a high-voltage operation is shown. Usually, Schottky contacts on either n- or p-type Si are manufactured and investigated using DLTS, which limits the investigation on either only electron or hole traps, respectively. Furthermore, transferring this knowledge to p+/n- diodes is not straight forward, as processing differences between Schottky and pn-diodes might lead to different defect levels and concentrations. For this reason, we performed capacitance-voltage (CV), current-voltage (IV), and DLTS measurements on the same p+/n- diodes to explain how Pt–H defects influence the device performance.

The annealing of Pt–H defects at temperatures above 550 K is known since 1997,<sup>[16]</sup> but there is little information on the activation energy for dissociation found in the literature. In case of Pt doping, Pt–H is the thermally most stable defect, which is in contrast with other TM such as Pd, Ag, or Au, where higher order TM–H<sub>x</sub> are most stable.<sup>[5]</sup> As we are able to anneal Pt–H defects, we can change its concentration and investigate how the diode characteristics in a reverse direction are influenced by gradually decreasing its concentration.

## 1. Introduction and Motivation

In silicon p+/n- diodes, Pt can be intentionally brought into the Si crystal via surface deposition and subsequent indiffusion<sup>[1–4]</sup> to control the minority carrier lifetime and thus the reverse recovery charge. However, hydrogen is also introduced into the Si crystal as a byproduct of various process steps, e.g., wet chemical etching<sup>[5,6]</sup> and further information is provided by Weber.<sup>[7,8]</sup> This causes

---

F. Rasinger, J. Prohinig, Dr. G. Pobegen  
KAI Kompetenzzentrum Automobil- und Industrieelektronik GmbH  
9524 Villach, Austria  
E-mail: fabian.rasinger@k-ai.at

F. Rasinger  
Lehrstuhl für Angewandte Physik, Department Physik  
Friedrich-Alexander University Erlangen-Nürnberg  
91058 Erlangen, Germany

J. Prohinig  
Institute of Solid State Physics  
University of Technology  
8010 Graz, Austria

Dr. H. Schulze  
Infineon Technologies Austria AG  
9500 Villach, Austria

Dr. H.-J. Schulze  
Infineon Technologies AG  
85579 Neubiberg, Germany

 The ORCID identification number(s) for the author(s) of this article can be found under <https://doi.org/10.1002/pssa.201900197>.

DOI: 10.1002/pssa.201900197

## 2. Samples

Fully processed high voltage (HV) p+/n- diodes with and without field stop (FS) regions, both with a doping concentration  $N_D$  of approximately  $10^{14} \text{ cm}^{-3}$ , are investigated. These diodes undergo exactly same processing steps, except in one diode the proton implantation processes from the backside generating the FS is skipped. The FS effect is created by higher n-type doping via the formation of shallow hydrogen-related donors.<sup>[17,18]</sup> Furthermore, a state-of-the-art edge termination protects the edges and corners of the anode against high electric fields

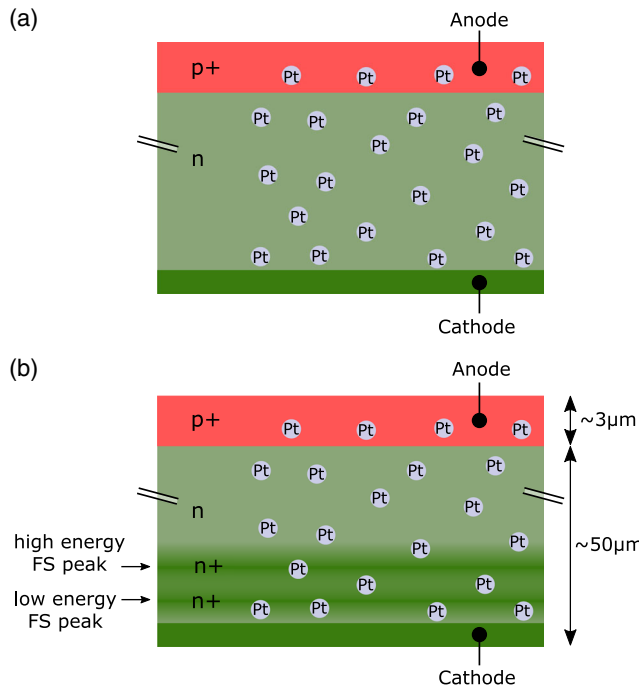


**Figure 1.** The schematic cross-section of a p+/n<sup>-</sup> diode with Pt doping displaying the diode with and without FS implantation at the backside. a) p+/n<sup>-</sup> diode without FS; b) p+/n<sup>-</sup> diode with FS implantation.

and enables reliable reverse current investigations up to high voltages. All samples are intentionally doped with Pt for minority carrier lifetime reduction, which leads to lower reverse recovery charge during turn-off. A schematic cross-section of the diode without and with FS implantation is shown in **Figure 1**. The edge termination is not sketched in this figure.

### 3. Experimental Section

#### 3.1. Precharacterization

We performed CV, HV IV, and DLTS measurements on p+/n<sup>-</sup> diodes with and without FS implantation and observed drastic differences in the diode performance especially in a reverse operation. The CV measurements showed exactly the same characteristics, which means that there was no difference in the shallow donor concentration  $N_D$  close to the pn-junction. Interestingly, the sample with additional FS implantation was found to have a smaller reverse current throughout the reverse characteristics in comparison with the sample without FS, as shown in **Figure 2a**. The avalanche breakdown started at approximately -500 V. In the DLTS measurements, the pulse and recovery voltage were chosen as  $V_p = 1$  V and  $V_{rec} = -10$  V, respectively. The pulse duration was set to  $t_p = 10$  ms, which was sufficient for the completion of trap filling. The first sampling point was at  $t_0 = 1.3$  ms, and the time window length was equal to  $T_w = 97.8$  ms.

Additional proton implantation was expected to generate Pt-H complexes that can be investigated via capacitance transient spectroscopy. DLTS measurements showed three main trapping levels: E(105), H(160), and E(240), which corresponded to a

single acceptor level Pt<sup>-/0</sup> ( $E_C - E_T = 0.23$  eV), a single donor level Pt<sup>0/+</sup> ( $E_V - E_T = 0.36$  eV) and an additional acceptor level identified as Pt-H defect ( $E_C - E_T = 0.50$  eV),<sup>[10,16]</sup> respectively.

$E_C$ ,  $E_V$ , and  $E_T$  denoted the energy position of the conduction band, the valence band, and of the trap level, respectively. Figure 2b shows the comparison between diode samples with and without FS.

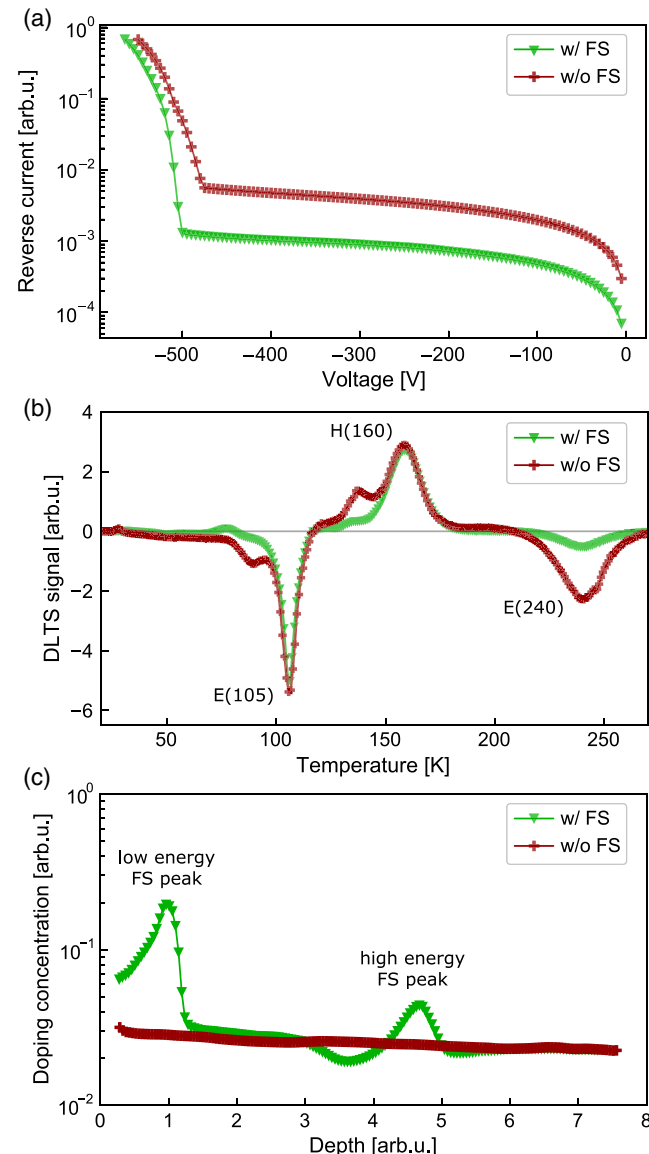


**Figure 2.** A precharacterization consisting of the reverse characteristic, the DLTS spectra, and the SRP profile from the backside of the diode with and without FS is conducted. a) Reverse characteristics up to avalanche breakdown of HV p+/n<sup>-</sup> diodes with and without FS. b) DLTS spectra of p+/n<sup>-</sup> diodes with and without FS, in which main peaks are named as E(105), H(160) and E(240) corresponding to single trap levels within the Si band gap. c) SRP profiles of the diode with and without FS showing the doping concentration with respect to depth measured from the backside in arbitrary units (arb. u.).

In the diode with FS, the total number of DLTS peaks was less, considering the smaller peaks at 90 and 140 K. Most significant was that there was a much smaller DLTS signal of the E(240) level that was measured in the diode with FS. We assumed that due to the formation of shallow H-related donors,<sup>[17]</sup> hydrogen was consumed by this defect, which left less H available for the Pt-H defects.<sup>[19]</sup> Another possible explanation is that the diffusion of hydrogen introduced from the backside was hindered due to the crystal damage of the FS implantation. Smaller peaks at 90 and 140 K were believed to be higher order Pt-H<sub>x</sub> complexes, as they were present in a higher extent in the diode that also suffered from higher Pt-H defect concentration. However, their trap concentration and activation energy were not easily evaluated due to much larger neighboring peaks and their presence nearly disappeared in the diode with FS. For this reason, we focused our investigations on the E(240) defect, which was electrically active and present in the middle of the silicon bandgap.

### 3.2. Spreading Resistance Profiling

Further insight into the n-doping generated by the FS implantation was given by spreading resistance profiling (SRP) from the backside of the diodes. The SRP profiles of the p+/n- diode with and without FS are shown in Figure 2c. At the FS peak, the shallow doping density clearly increased in the p+/n- diode with FS. One FS peak corresponded to a certain proton beam energy and fluence. The sample without FS implantation naturally showed no change in the n-type doping concentration  $N_D$  with respect to depth.

### 3.3. Annealing Series

According to Sachse et al.,<sup>[16]</sup> the Pt-H defect can be dissociated at temperatures above 550 K; thus, we performed an annealing series in a conventional furnace using N<sub>2</sub> ambient with both samples simultaneously. The thermal budget varied via the annealing temperature that was between  $T_0$  and  $T_0 + 100$  K and via time that ranged from 5 to 900 min. It was believed that a dissociation reaction of the Pt-H defect took place, where hydrogen was diffusing away and the substitutional Pt was left behind. The first observation after annealing was a decrease in reverse current of approximately one order of magnitude in both samples. Furthermore, the Pt-H defect disappeared after annealing at  $T_0 + 30$  K for 10 h, as shown ideally for diodes without FS in Figure 3. The focus in the following investigation was set on the E(240) peak assigned to the Pt-H defect.<sup>[10]</sup>

The trap concentrations of the E(240) defect in the p+/n- diodes without and with FS are shown in Figure 4a and b, respectively. A dissociation reaction of first order was assumed to model the behavior with respect to the annealing temperature  $T$  and time  $t$ , assuming that only one defect species A reacts. The defect concentration [A] is given as a function of  $t$  and  $T$  by

$$[A](t, T) = [A_0] \exp\left(-c_0 \exp\left(-\frac{E_A}{kT}\right)t\right) \quad (1)$$

where  $[A_0]$  is the initial defect concentration. The reaction rate constant  $c_0$  and the activation energy  $E_A$  are fitting parameters.

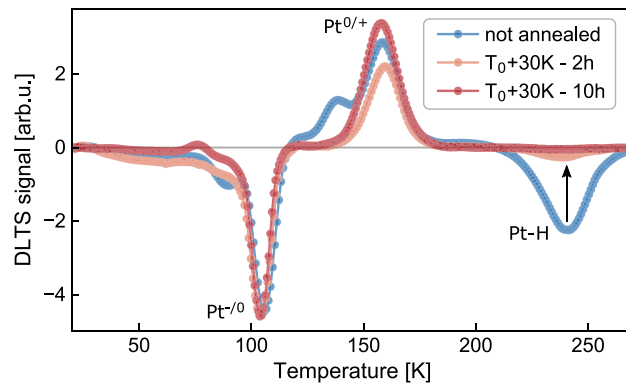


**Figure 3.** DLTS spectra of p+/n- diodes without FS not annealed in comparison with annealed samples at  $T_0 + 30$  K for 2 and 10 h. The arrow indicates the decrease of the assigned Pt-H defect.

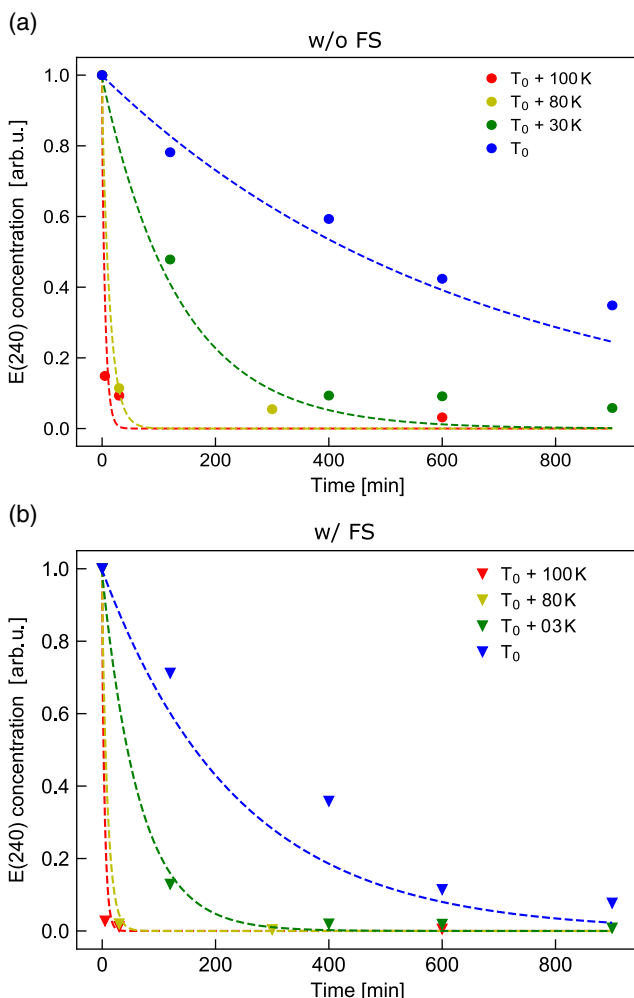


**Figure 4.** Annealing series of the diode with and without FS. A first-order dissociation model is fitted (dashed lines). a) p+/n- diodes without FS; b) p+/n- diodes with FS.

As heating and cooling in the used oven took several minutes, we included the thermal budget when evaluating the annealing series. For this reason, we included a heating ramp of  $6\text{ K min}^{-1}$  and a cooling ramp of  $5\text{ K min}^{-1}$  into the model. A curve fitting algorithm was utilized, in which the concentration  $[A]$  was a function of annealing temperature as well as time to obtain the activation energy  $E_A$  and its uncertainty. The experimental data of the annealing series are fitted as

$$E_{A,\text{w/FS}} = (1.5 \pm 0.4) \text{ eV} \quad (2)$$

and

$$E_{A,\text{w/oFS}} = (1.2 \pm 0.5) \text{ eV} \quad (3)$$

for the diode with and without FS, respectively. Obviously, the reaction was not significantly influenced by the additional FS implantation.

### 3.4. Impact on Reverse Characteristic

Furthermore, we find a clear impact of the annealed E(240) defect on reverse characteristic of the HV p+/n- diodes. The reverse current was drastically lowered in samples that experienced higher thermal budget. The reverse current can be split into two main components: the diffusion and the generation current.<sup>[20]</sup> As the generation current was linearly increased with the space charge region width  $x$ , these two components can be separated. Hazdra et al.<sup>[21]</sup> applied the following equation

$$N_T(x) = \frac{1}{q\xi} \frac{dJ}{dx} \quad (4)$$

to calculate depth profiles of the divacancy defect  $V_2^{-1/0}$ , which was the main generation center in their diodes. This equation can also be applied to other generation centers lying in the middle of the silicon bandgap. It described how the derivative of the reverse current density  $J$  with respect to the space charge region depth  $x$  was directly proportional to the trap concentration  $N_T(x)$  at a certain depth. The proportionality constants were the elementary charge  $q$  and the emissivity of the defect  $\xi$ . With constant shallow doping concentration  $N_D$  throughout the diode, the space charge depth  $x$  was calculated using the equation for an abrupt one-sided p+/n- junction<sup>[21]</sup>

$$x = \sqrt{\frac{2\varepsilon_0\varepsilon_r(V_r - V_{bi})}{qN_D}} - \lambda \quad (5)$$

The vacuum permittivity and the relative permittivity of the semiconductor are denoted  $\varepsilon_0$  and  $\varepsilon_r$ , respectively. The applied reverse voltage  $V_r$  minus the built-in voltage  $V_{bi}$  continuously increased the space charge region depth  $x$ . The  $\lambda$ -correction<sup>[22]</sup> was introduced to calculate the trap depth more exactly. The space charge region length was reduced for a certain length  $\lambda$ , which accounted for the intersection of the Fermi-level with the trap level. For the calculation of the derivative  $dJ/dx$ , the  $\lambda$ -correction was not relevant, as  $\lambda$  was not dependent on  $V_r$ .

Equation (4) is only valid, if one defect is mainly responsible for the generation current. Otherwise, several trap levels and

their corresponding emissivities have to be taken into account. To check the number of different defects in our devices, we measured the reverse characteristic and the DLTS spectrum on the same p+/n- diode for all the performed annealing steps. In Figure 5, the  $N_T$  measured via DLTS versus  $dJ/dx$  obtained in IV characteristics close to the p+/n- junction is shown. We found a strictly linear correlation showing that the level E(240) was the main generation center in these diodes. As the recovery voltage and the pulse voltage in the DLTS measurement were chosen as  $-10$  and  $0\text{ V}$ , respectively, the generation current had to be evaluated within this voltage range. The fit of a linear function without y-intercept (dashed black line) gives a universal emissivity for the E(240) level of  $\xi = 450\text{ s}^{-1}$  and proves that this level is mainly responsible for high reverse currents.

### 3.5. Depth Profiles

We further used Equation (5) to obtain a depth profile of the E(240) level, which was not easily possible by DLTS, as a high reverse bias up to  $500\text{ V}$  for these diodes is needed. Therefore, we derived the reverse current with respect to the space charge region width throughout the reverse characteristic, assuming a constant doping density with respect to depth. This calculation gives a quantification of the generation-related current as a function of depth. Alternatively, the x-axis can be transformed to reverse voltages to find out at which voltage level the FS is depleted. Using DLTS, we check whether the relation  $N_T < N_D$  for the E(240) level is satisfied close to the p+/n- junction and further assure that this is valid throughout the thickness of the diode. We found that this relation was fulfilled for all the investigated samples. Figure 6a shows how annealing at  $T_0 + 30\text{ K}$  decreases the E(240) level with higher annealing durations (see the 120 min and the 600 min curve). In addition, it was found that the derivative and so the E(240) level in the not-annealed sample increased slightly with depth. Therefore, we

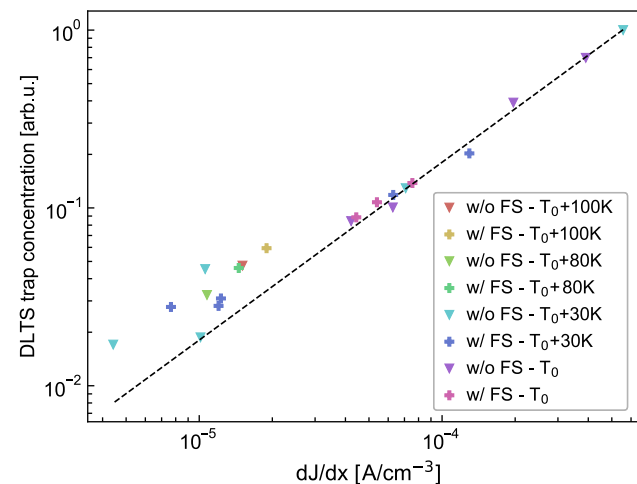


**Figure 5.** Defect concentration  $N_T$  of E(240) versus the derivative of reverse current density with respect to the space charge region width  $dJ/dx$ . The dashed line represents the slope for an universal emissivity  $\xi$  of  $450\text{ s}^{-1}$ .

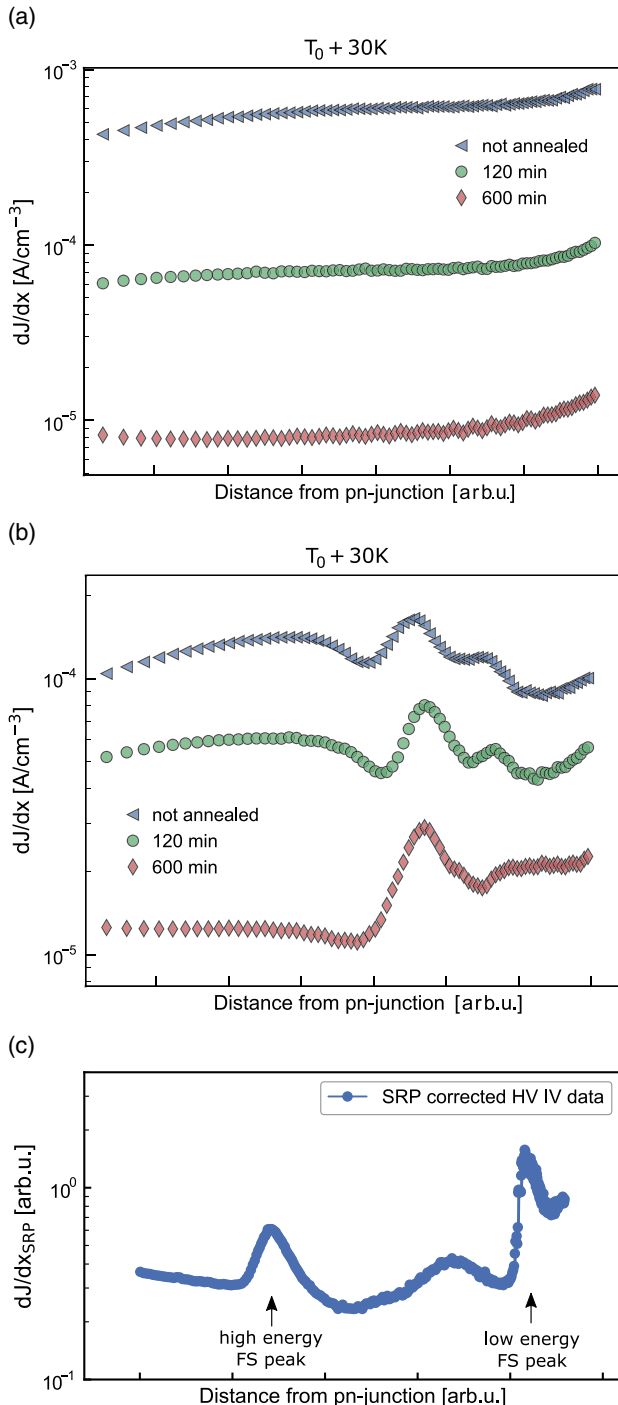


**Figure 6.** a,b) The derivative  $dJ/dx$  is giving a measure for the E(240) trap concentration as a function of the distance from the p+/n- junction. A comparison of the 120 min, the 600 min, and the not-annealed sample is depicted. c) The derivative  $dJ/dx_{SRP}$  from HV IV data are corrected using the doping concentration from the SRP data as a function of the distance from the pn-junction. a) p+/n- diode without FS implantation; b) p+/n- diode with FS implantation; c) p+/n- diode with FS implantation (not annealed).

concluded that hydrogen was probably introduced via a backside process. The increasing derivative at the end of the depth profile

was likely a field-induced generation current, as it was visible in all samples.

Furthermore, Figure 6b shows the derivative of the reverse current density of the diode with FS. In the first approximation, a constant doping with respect to depth was assumed. Two regions were clearly identified. First, close to the p+/n- junction, there was a rather constant derivative that was similar to the sample without FS. Second, near the backside, there was a strong change of the derivative with depth. This effect can be explained by the FS implantation, which locally increased the donor doping concentration in the n-type material. In addition, the FS implantation might create additional defects, which were acting as the generation centers and thus increased the derivative of the reverse current density.

A corrected depth profile of the diode with FS (not annealed) was calculated using the reverse HV IV data and the SRP data and is shown in Figure 6c. As the FS implantation increased the shallow donor concentration close to the backside of the diode, the approximation of constant doping  $N_D$  was not valid anymore. Therefore, the SRP data together with Poisson's equation were utilized to obtain the space charge region depth  $x_{SRP}$  as a function of the applied reverse voltage. The distance from the pn-junction was only shifted slightly, but the derivative with respect to  $dx_{SRP}$  changed significantly. This correction was used to numerically calculate the  $dx_{SRP}$  for the  $dJ/dx_{SRP}$  curve. At the depth of the first peak in the  $dJ/dx_{SRP}$  curve, there was also a peak in the doping concentration curve (high-energy FS peak). At a larger distance from the pn-junction, a small, additional peak followed, whereby its origin was likely caused by the low-energy FS peak. The highest peak in the  $dJ/dx_{SRP}$  curve close to the backside was clearly due to the low-energy FS implantation.

#### 4. Conclusion

By utilizing DLTS measurements, three main trap levels are investigated and assigned to their microscopic defect origin. In detail, these trap levels are called E(105), H(160), and E(240), which correspond to  $Pt^{-/0}$ ,  $Pt^{0/+}$ , and the Pt-H defects, respectively. The Pt-H level is found in Pt-doped silicon p+/n- diodes at a higher concentration throughout the device in samples without FS compared with samples with FS. This defect is likely introduced from the backside via a hydrogen-incorporating process. The influence of this defect on the reverse current characteristics of the p+/n- diode is demonstrated. As the Pt-H defect is a major generation center, which is proven by plotting  $dJ/dx$  versus the trap concentration  $N_T$ ; it continuously increases the current when increasing the reverse voltage. However, as already reported in the literature, this defect dissociates at annealing temperatures higher than 550 K,<sup>[16]</sup> which we are able to verify. The dissociation energy is independent of the FS implantation and is obtained as  $E_{A,w/FS} = (1.5 \pm 0.4)$  eV and  $E_{A,w/oFS} = (1.2 \pm 0.5)$  eV, respectively. In addition, the depth profiles are calculated via the derivative of the reverse current with respect to space charge width  $dJ/dx$ , which gives a quantification of the generation-related current. In diode samples with FS implantation, the constant doping assumption is not valid anymore, but the SRP data can be utilized to correct the  $dJ/dx$  profile. The presented results show the impact of Pt-H

defects on reverse characteristics of high voltage p+/n<sup>-</sup> diodes and its controllability via annealing in a conventional furnace using N<sub>2</sub> atmosphere.

## Acknowledgements

This work was funded by the Austrian Research Promotion Agency (FFG, Project No. 863947). The authors would further like to thank Johannes Zechner and Sebastian Moser (both KAI Kompetenzzentrum Automobil- und Industrieelektronik GmbH) for enabling and performing the annealing experiment.

## Conflict of Interest

The authors declare no conflict of interest.

## Keywords

annealing study, capacitance–voltage, current–voltage characteristics, deep-level transient spectroscopy, high voltage p+/n<sup>-</sup> diode, platinum–hydrogen defects

Received: March 18, 2019

Revised: May 10, 2019

Published online: July 5, 2019

- [1] E. Badr, P. Pichler, G. Schmidt, in Ph. D. Research in Microelectronics and Electronics (PRIME), 2013 9th Conf. on, IEEE **2013**, pp. 253–256.
- [2] E. Badr, P. Pichler, G. Schmidt, *J. Appl. Phys.* **2014**, *116*, 133508.
- [3] A. Johnsson, P. Pichler, G. Schmidt, *Phys. Status Solidi (a)* **2017**, *214*, 1700207.
- [4] M. Hauf, C. Sandow, F. J. Niedernostheide, G. Schmidt, in 2018 IEEE 30th Int. Symp. on Power Semiconductor Devices and ICs (ISPSD), IEEE **2018**, pp. 120–123.

- [5] J. U. Sachse, E. Sveinbjörnsson, N. Yarykin, J. Weber, *Mater. Sci. Eng., B* **1999**, *58*, 134.
- [6] E. Badr, P. Pichler, G. Schmidt, in *Solid State Phenomena*, Trans Tech Publications **2014**, pp. 260–264.
- [7] J. Weber, in Crystalline Defects and Contamination: Their Impact and Control in Device Manufacturing III: DECON 2001: Proc. of the Satellite Symp. to ESSDERC 2001, Nuremberg, Germany **2001**, p. 53.
- [8] J. Weber, *Phys. Status Solidi c* **2008**, *5*, 535.
- [9] M. Weirstein, M. Stavola, K. L. Stavola, S. Uftring, J. Weber, J. U. Sachse, H. Lemke, *Phys. Rev. B* **2001**, *65*, 035206.
- [10] J. U. Sachse, J. Weber, E. Sveinbjörnsson, *Phys. Rev. B* **1999**, *60*, 1474.
- [11] S. Knack, J. Weber, H. Lemke, H. Riemann, *Phys. Rev. B* **2002**, *65*, 165203.
- [12] N. Yarykin, J. U. Sachse, H. Lemke, J. Weber, *Phys. Rev. B* **1999**, *59*, 5551.
- [13] J. U. Sachse, J. Weber, H. Lemke, in *Materials Science Forum*, Trans Tech Publications **1997**, pp. 307–312.
- [14] W. Jost, Dissertation, University of Stuttgart, **1996**.
- [15] R. Jones, A. Resende, S. Öberg, P. Briddon, *Mater. Sci. Eng., B* **1999**, *58*, 113.
- [16] J. U. Sachse, E. Sveinbjörnsson, W. Jost, J. Weber, H. Lemke, *Phys. Rev. B* **1997**, *55*, 16176.
- [17] F. J. Niedernostheide, H. J. Schulze, H. Felsl, F. Hille, J. Laven, M. Pfaffenlehner, C. Schäffer, H. Schulze, W. Schustereder, in 28th Int. Symp. on Power Semiconductor Devices and ICs (ISPSD), IEEE **2016**, pp. 351–354.
- [18] I. Grekhov, L. Kostina, V. Lomasov, S. A. Yusupova, E. Belyakova, *Tech. Phys. Lett.* **2014**, *40*, 1069.
- [19] J. Prohlinig, F. Rasinger, H. J. Schulze, G. Pobegen, in 2018 Int. Semiconductor Conf. (CAS), IEEE **2018**, pp. 223–226.
- [20] Y. Murakami, T. Shingyouji, *J. Appl. Phys.* **1994**, *75*, 3548.
- [21] P. Hazdra, J. Rubeš, J. Vobecký, *Nucl. Instrum. Methods Phys. Res., Sect. B* **1999**, *159*, 207.
- [22] D. Lang, *Thermally Stimulated Relaxation in Solids*, Springer, Berlin/New York **1979**, pp. 93–133.